Electronic Supplementary Information (ESI)

Achieving Strong Second Harmonic Generation Effects Induced by Dimensional Increase of PbX_6 Octahedron and Halogen Substitute of $(C_{10}H_{11}N_3)PbX_4$ （X = Cl, Br）

Li-Ling Zhang [1], Qingran Ding [1*], Peihan Wang [2], Yanqiu Zhang [1], Qing-Yan Liu [1*], Yu-Ling Wang [1*] & Junhua Luo [1,3]

[1]College of Chemistry and Chemical Engineering, Key Lab of Fluorine and Silicon for Energy Materials and Chemistry of Ministry of Education and National Engineering Research Centre for Carbohydrate Synthesis, Jiangxi Normal University, Nanchang 330022, Jiangxi. [2]School of Materials Science and Engineering, Frontiers Science Center for New Organic Matter, Nankai University, Tianjin 300350. [3]State Key Laboratory of Structural Chemistry, Fujian Institute of Research on the Structure of Matter, Chinese Academy of Sciences, Fuzhou, Fujian 350002.

Corresponding Authors (email: dqr@jxnu.edu.cn; qyliuchem@jxnu.edu.cn; ylwang@jxnu.edu.cn)

1. Characterization.

X-Ray Single Crystal Structure Determination. X-ray single-crystal diffraction experiments were carried out a Rigaku Oxford SuperNova or XtaLAB Synergy R diffractometer (Mo-K*a* radiation, λ = 0.71073 Å). Absorption correction and data reduction were handled with a *CrysAlisPro package*.[1] The *SHELXT* [2] and *SHELXL* [3] were applied to structure solution and refinement, respectively. The hydrogen atoms were added theoretically. Non-hydrogen atoms were refined anisotropically. Details of crystal parameters, data collection, and structure refinement are summarized in Table S1. The important bond lengths and bond angles are listed in Table S2 and S3. Hydrogen bonds are listed in Table S4.

Powder XRD Analysis. Powder X-ray diffraction measurements of the $(C_{10}H_{11}N_3)PbX_4$ (X=Cl, Br) sample was carried out with a Miniflex 600 diffractometer equipped with an incident beam monochromator set for Cu Kα radiation (λ= 1.5418 Å). The 2θ range was 5-75 °with a scan step width of 0.02 °and a fixed counting time of 0.15s/step.

Thermal Stability. Thermal gravimetric analysis (TGA) carried out on a NETZSCH STA 449 thermogravimetric analyzer. About 8.5 mg of $(C_{10}H_{11}N_3)PbCl_4$ and 10.2 mg of $(C_{10}H_{11}N_3)PbBr_4$ samples was placed in Al_2O_3 crucibles, which were heated at a rate of 10 K min^{-1} from room temperature to 800 K, and then cooled to room temperature at the same rate under flowing nitrogen.

UV-Vis-NIR Diffuse. The UV-vis-NIR diffuse reflection data was recorded at room temperature using $BaSO_4$ powder sample as a standard (100% reflectance) on a PerkinElmer Lamda-950 UV/vis/NIR spectrophotometer (scanning wavelength is between 200 and 800 nm).

Second-Harmonic Generation. Powder second-harmonic generation measurements were carried out by the Kurtz-Perry method.[4] The measurements were performed with a Q-switched Nd: YGA laser at a wavelength of 1064 nm. Since SHG efficiency has significant correlation with the particle size of crystal, the sample was ground and sieved into the following particle size ranges: 25-45 μm, 45-53 μm, 53-75 μm, 75-105 μm, 105-150 μm, 150-210 μm, 210-300 μm. Then the samples of different particle sizes were pressed between two rounded 1 mm thick sheet glasses with a 2 mm thick rubber ring interlayer containing an 8 mm diameter hole in the middle, which were tightly sheathed in an aluminous round box with an 8 mm diameter hole in the middle. Relevant comparisons had been made with the well-known SHG material KDP by grinding and sieving into the same particle size ranges. The measurements were performed on a 1064 nm Q-switched Nd: YAG laser under the same voltage. The ratio of the second-harmonic intensity outputs was calculated.

The SHG measurements of single-crystals were carried out using a home-built multiphoton nonlinear optical microscope system.[5] A commercial femotosecond pump (Mai Tai HP, wavelength ranging from 690 to 1040 nm) was used in the reflection geometry with incidence and detection angles both of 45 degree. The linearly polarized pump was altered with the λ/2 plate. The reflected SHG signal is received from the front surface of crystals. The linearly polarized dependent SHG signals were collected every 10 degrees. Power dependent SHG measurements were collected upon 900 nm laser excitation with increasing laser power. The laser spot was about 20 μm in diameter. The pulse width was ~100 fs. The frequency was 80 MHz. The KDP is used as a benchmark for SHG signal intensity.

Birefringence Measurement. The Birefringence of $(C_{10}H_{11}N_3)PbX_4$ (X=Cl, Br) was obtained through a polarizing microscope (Nikon LV1000) equipped with a Berek compensator at a

wavelength of 550 nm. Small crystals were chosen for the measurements. The following formula was listed to calculate birefringence: $R = |N_e\text{-}N_o| = \Delta n \times T$, where R denotes the optical path difference, Δn represents birefringence, and T denotes the thickness of the crystal.

Computational Methods. The first-principles calculations for $(C_{10}H_{11}N_3)PbX_4$ (X=Cl, Br) were performed by CASTEP [6] on a plane-wave pseudopotential total energy package based density functional theory (DFT).[7] The functional developed by Perdew-Burke-Ernzerhof (PBE) functional within the generalized gradient approximation (GGA)[8,9] form was adopted to describe the exchange-correlation energy. The ultrasoft pseudopotentials were used to model the effective interaction between atom cores and valence electrons. H $1s^1$, C $2s^22p^2$, N $2s^22p^3$, Cl $3s^23p^5$, Br $4s^24p^5$ and Pb $6s^26p^2$ electrons were treated as valence electrons. The kinetic energy cutoff of 380 eV and dense 2 × 2 × 1 Monkhorst-Pack[10] k-point meshes in the Brillouin zones were chosen. The linear optical properties were examined based on the dielectric function $\varepsilon(\omega) = \varepsilon_1(\omega) + i\varepsilon_2(\omega)$. The imaginary part of dielectric function ε_2 can be calculated based on the electronic structures and the real part is obtained by the Kramers-Kronig transformation, accordingly the refractive indices and the birefringence (Δn) can be calculated. The frequency-dependent refractive indices were calculated to demonstrate the validity of birefringence measurements.

Table S1. Crystal data and structural refinement data.

	$(C_{10}H_{11}N_3)PbCl_4$	**$(C_{10}H_{11}N_3)PbBr_4$**
Empirical formula	$C_{10}H_{11}N_3Cl_4Pb$	$C_{10}H_{11}N_3Br_4Pb$
CCDC	2310909	2310914
Formula mass	522.21	700.05
Temperature (K)	293	284(2)
Crystal system	monoclinic	monoclinic
Space group	*Cc*	*Cc*
a (Å)	4.2699(2)	4.41520(10)
b (Å)	23.1667(11)	23.9772(6)
c (Å)	15.0175(8)	15.2356(4)
α (°)	90	90
β (°)	97.952(5)	97.245(2)
γ (°)	90	90
V ($Å^3$)	1471.24(13)	1600.03(7)
Z	4	4
ρ (calculated) (g cm^{-3})	2.358	2.9059
F(000)	968	1256
Reflections collected	4663	12085
Goodness-of-fit on F^2	1.007	1.055
Final *R* indexes [$I>=2\sigma(I)$]	R_1 = 0.0251 wR_2 = 0.0548	R_1 = 0.0267 wR_2 = 0.0712
Final *R* indexes [all data]	R_1 = 0.0263 wR_2 = 0.0554	R_1 = 0.0282 wR_2 = 0.0715
Flack parameter	0.044(9)	– 0.016(6)

Table S2. Selected bond lengths (Å) and angles ( ) for $(C_{10}H_{11}N_3)PbCl_4$ (**1**).

Selected bond lengths			
Pb1–Cl1	2.801(2)	Pb1–Cl3	2.884(2)
Pb1–Cl4	2.841(2)	Pb1–Cl1$^{\#1}$	3.084(2)
Pb1–Cl2	2.818(2)	Pb1–Cl2$^{\#1}$	3.081(2)
Selected bond angles			
Cl1–Pb1–Cl4	87.39(7)	Pb1–Cl2–Pb1$^{\#2}$	92.63(6)
Cl1–Pb1–Cl2	92.11(7)	Cl1–Pb1–Cl2$^{\#1}$	173.43(7)
Cl4–Pb1–Cl2	85.70(8)	Cl4–Pb1–Cl2$^{\#1}$	97.49(7)
Cl1–Pb1–Cl3	82.87(7)	Cl2–Pb1–Cl2$^{\#1}$	92.63(7)
Cl4–Pb1–Cl3	166.06(8)	Cl2–Pb1–Cl3	84.72(7)
Cl3–Pb1–Cl2$^{\#1}$	93.05(7)	Cl2–Pb1–Cl1$^{\#1}$	173.25(7)

symmetry Codes: #1, –1+*x*, *y*, *z*; #2, 1+*x*, *y*, *z*.

Table S3. Selected bond lengths (Å) and angles (°) for $(C_{10}H_{11}N_3)PbBr_4$ (**2**).

Selected bond lengths			
Pb1–Br4	2.9459(11)	Pb1–Br3	3.0401(10)
Pb1–Br1	2.9576(10)	Pb1–Br1$^{\#1}$	3.1720(10)
Pb1–Br2	2.9637(9)	Pb1–Br2$^{\#1}$	3.1859(10)
Selected bond angles			
Br4–Pb1–Br1	87.08(3)	Br4–Pb1–Br1$^{\#1}$	96.89(3)
Br4–Pb1–Br2	86.86(3)	Br1–Pb1–Br1$^{\#1}$	92.09(3)
Br1–Pb1–Br2	91.93(3)	Br2–Pb1–Br1$^{\#1}$	174.63(3)
Br4–Pb1–Br3	166.80(3)	Br3–Pb1–Br1$^{\#1}$	92.16(3)
Br1–Pb1–Br3	82.99(3)	Pb1–Br2–Pb1$^{\#2}$	91.70(3)
Br2–Pb1–Br3	84.81(3)	Br2–Pb1–Br1	174.93(3)

symmetry Codes: #1, 1+*x*, *y*, *z*; #2, –1+*x*, *y*, *z*.

Table S4. The parameters of the hydrogen bonds for $(C_{10}H_{11}N_3)PbCl_4$ (1) and $(C_{10}H_{11}N_3)PbBr_4$ (**2**).

D–H ···A	D–H (Å)	H ···A (Å)	D ···A (Å)	<D–H ···A (°)
N1–H1 ···Cl1$^{\#1}$	0.86	2.65	3.315(10)	134.8
N2–H2 ···Cl4$^{\#2}$	0.86	2.25	3.104(9)	173.8
N3–H3 ···Cl3	0.86	2.46	3.215(8)	146.9
N1–H1 ···Br1$^{\#1}$	0.86	2.78	3.451(9)	135.6
N2–H2 ···Br4$^{\#2}$	0.86	2.38	3.232(9)	171.6
N3–H3 ···Br3	0.86	2.62	3.364(8)	144.9

2. Results and discussion

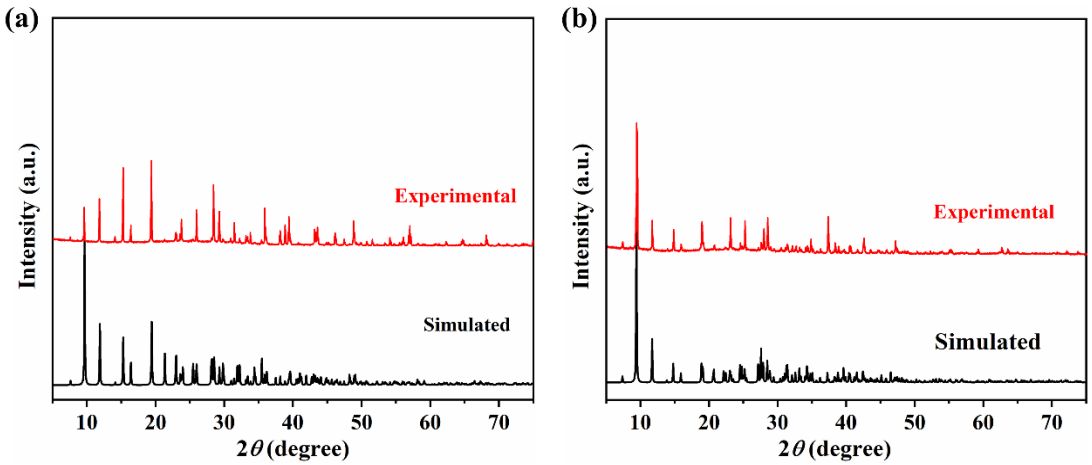

Fig. S1 (a) PXRD patterns of $(C_{10}H_{11}N_3)PbCl_4$ (**1**) and (b) $(C_{10}H_{11}N_3)PbBr_4$ (**2**).

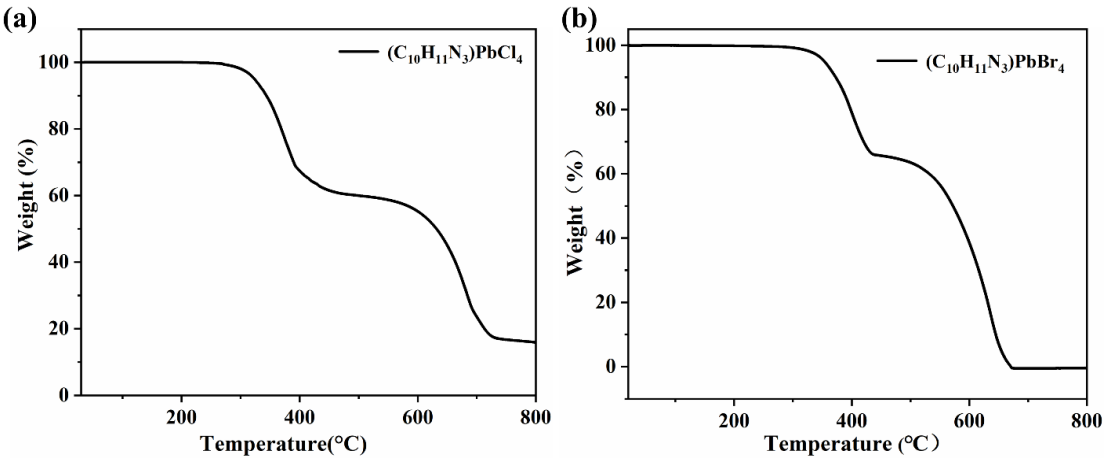

Fig. S2 (a) The thermal stability analysis of TG curves of $(C_{10}H_{11}N_3)PbCl_4$ (**1**) and (b) $(C_{10}H_{11}N_3)PbBr_4$ (**2**) under nitrogen atmosphere.

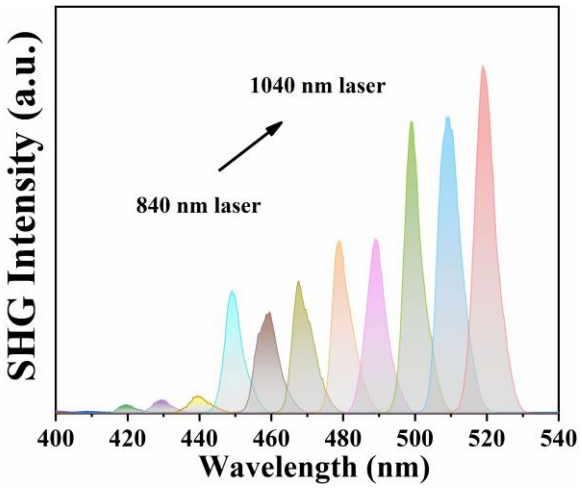

Fig. S3 SHG response of $(C_{10}H_{11}N_3)PbCl_4$ (**1**) crystal pumped at different wavelengths.

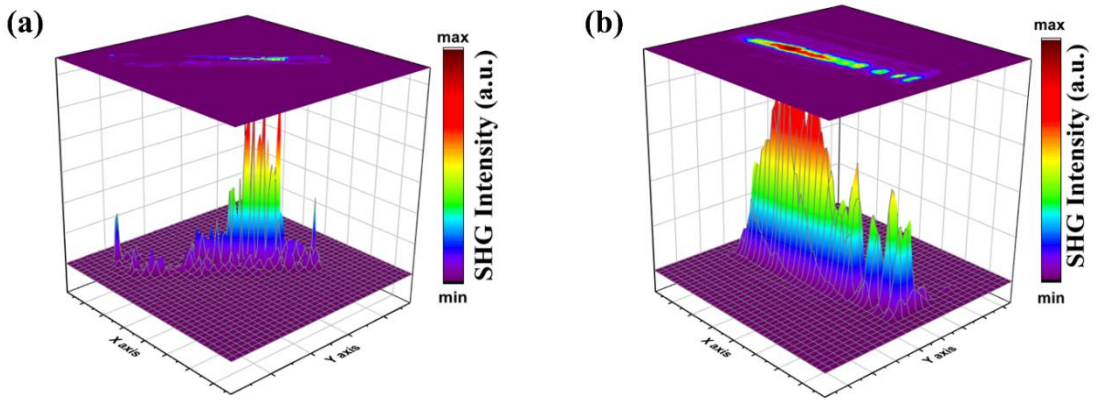

Fig. S4 Scanned images of a crystal of (a) $(C_{10}H_{11}N_3)PbCl_4$ (**1**) and (b) $(C_{10}H_{11}N_3)PbBr_4$ (**2**) by detecting the SHG signals (at 520 nm when pumped at 1040 nm) while scanning the samples.

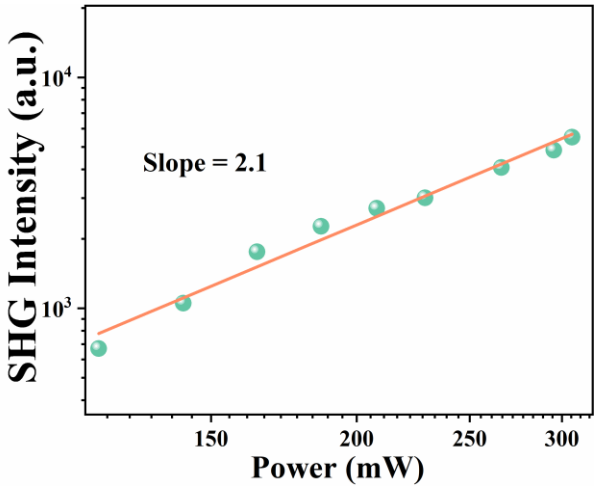

Fig. S5 Logarithmic plot of SHG intensity versus incident power for $(C_{10}H_{11}N_3)PbCl_4$ (**1**) (The orange line is the best linear fitting of the experimental data).

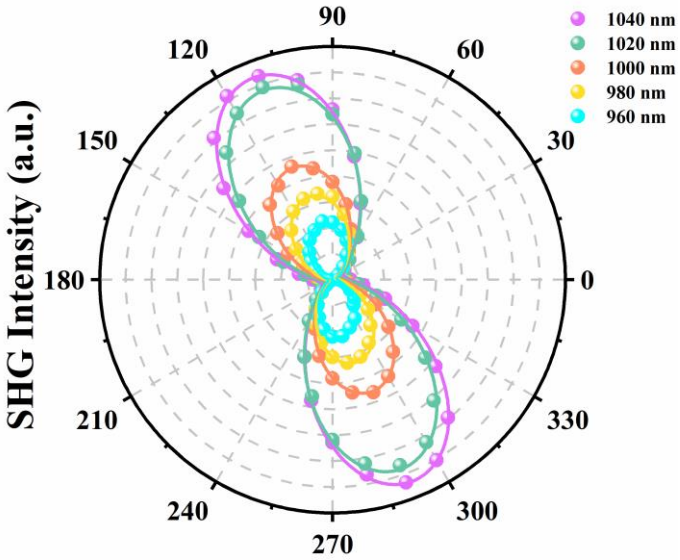

Fig. S6 SHG intensity of $(C_{10}H_{11}N_3)PbCl_4$ (**1**) at different linearly polarized angles and different laser wavelengths (The solid lines are the nonlinear fitting of the experimental data).

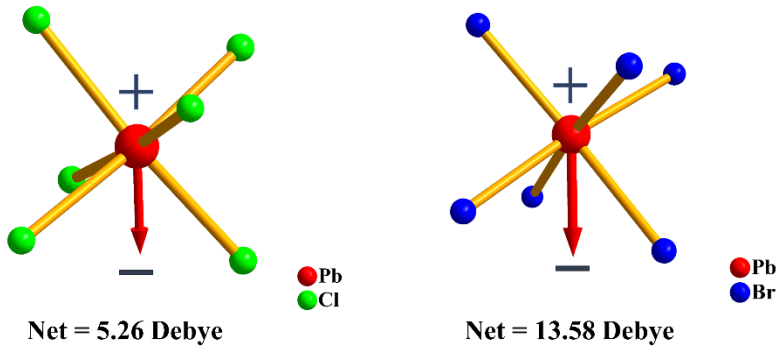

Fig. S7 Direction of the dipole moment vectors (red arrows) in the distorted $PbCl_6$ and $PbBr_6$ octahedrons in $(C_{10}H_{11}N_3)PbCl_4$ (**1**) and $(C_{10}H_{11}N_3)PbBr_4$ (**2**).

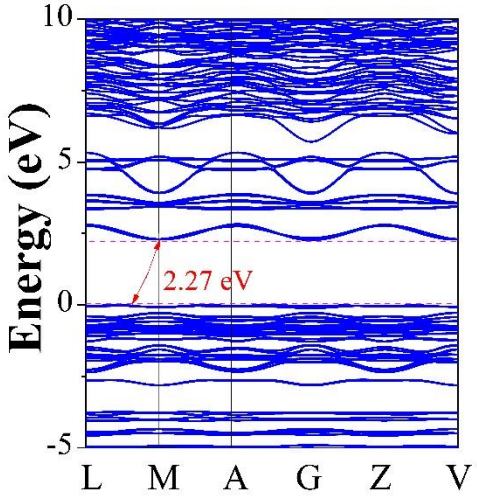

Fig. S8 Calculated energy band structures of $(C_{10}H_{11}N_3)PbCl_4$ (**1**).

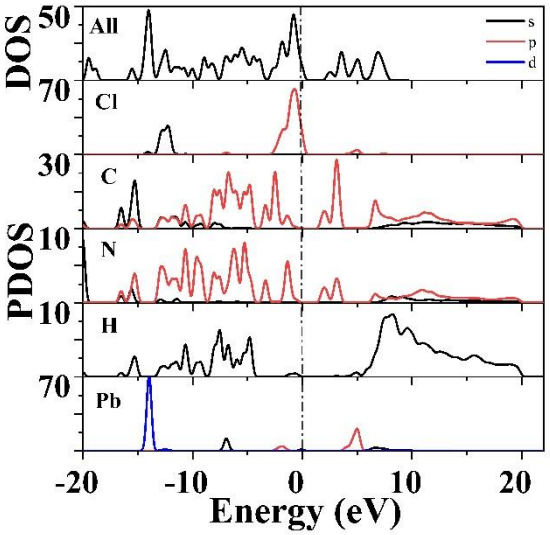

Fig. S9 DOS and PDOS of $(C_{10}H_{11}N_3)PbCl_4$ (**1**).

References

1 CrysAlisPro, Rigaku Oxford Diffraction: The Woodlands, TX. 2015.

2 G. M. Sheldrick, *Acta Crystallogr Sect C Struct Chem*, 2015, **C71**, 3–8.

3 G. M. Sheldrick, *Acta Crystallogr*, 2008, **A64**, 112–122.

4 S. K. Kurtz, and T. T. Perry, *J. Appl. Phys*, 1968, **39**, 3798–3813.

5 C. Yuan, X. Li, S. Semin, Y. Feng, T. Rasing and J. Xu, *Nano Lett*, 2018, **18**, 5411-5417.

6 S. J. Clark, M. D. Segall, C. J. Pickard, P. J. Hasnip, M. I. J. Probert, K. Refson and M. C. Payne, *Für Krist. - Cryst. Mater*, 2005, **220**, 567–570.

7 M. C. Payne, M. P. Teter, D. C. Allan, T. A. Arias and J. D. Joannopoulos, *Rev. Mod. Phys*, 1992, **64**, 1045–1097.

8 D. M. Ceperley and B. J. Alder, *Phys. Rev. Lett*, 1980, **45**, 566–569.

9 J. P. Perdew and A. Zunger, *Phys. Rev.* B, 1981, **23**, 5048–5079.

10 H. J. Monkhorst and J. D. Pack, *Phys. Rev.* B, 1976, **13**, 5188–5192.